Transp Porous Med (2011) 90:135–151
DOI 10.1007/s11242-011-9729-6

Numerical Simulation Studies of the Long-term Evolution of a CO_2 Plume in a Saline Aquifer with a Sloping Caprock

Karsten Pruess · Jan Nordbotten

Received: 9 December 2009 / Accepted: 12 January 2011 / Published online: 2 February 2011

Abstract We have used the TOUGH2-MP/ECO2N code to perform numerical simulation studies of the long-term behavior of CO_2 stored in an aquifer with a sloping caprock. This problem is of great practical interest, and is very challenging due to the importance of multi-scale processes. We find that the mechanism of plume advance is different from what is seen in a forced immiscible displacement, such as gas injection into a water-saturated medium. Instead of pushing the water forward, the plume advances because the vertical pressure gradients within the plume are smaller than hydrostatic, causing the groundwater column to collapse ahead of the plume tip. Increased resistance to vertical flow of aqueous phase in anisotropic media leads to reduced speed of up-dip plume advancement. Vertical equilibrium models that ignore effects of vertical flow will overpredict the speed of plume advancement. The CO_2 plume becomes thinner as it advances, but the speed of advancement remains constant over the entire simulation period of up to 400 years, with migration distances of more than 80 km. Our simulations include dissolution of CO_2 into the aqueous phase and associated density increase, and molecular diffusion. However, no convection develops in the aqueous phase because it is suppressed by the relatively coarse (sub-) horizontal gridding required in a regional-scale model. A first crude sub-grid-scale model was developed to represent convective enhancement of CO_2 dissolution. This process is found to greatly reduce the thickness of the CO_2 plume, but, for the parameters used in our simulations, does not affect the speed of plume advancement.

Keywords CO_2 plume · Long-term fate · Sloping aquifer · Numerical simulation · Enhanced dissolution · Capillary effects

K. Pruess (✉)
Earth Sciences Division, Lawrence Berkeley National Laboratory, Berkeley, CA, USA
e-mail: K_Pruess@lbl.gov

J. Nordbotten
Department of Mathematics, University of Bergen/Norway, Bergen, Norway

1 Introduction

Geologic storage as a greenhouse gas mitigation strategy will be workable only if long-term secure containment of CO_2 can be assured. At typical subsurface temperature and pressure conditions in terrestrial crust, separate-phase supercritical CO_2, henceforth for simplicity referred to as "gas," is less dense than aqueous phase. CO_2 injected into a saline aquifer will thus experience an upward buoyancy force, will tend to accumulate under a caprock, and will migrate toward shallower depth whenever suitable permeable pathways are available, such as fractures, faults, or improperly abandoned wells (Nordbotten et al. 2005; Pruess 2008; Celia et al. 2008).

Large potential for CO_2 geologic storage exists in sedimentary basins in which saline aquifers and associated caprock formations have significant slope that persists on regional scales. Important examples include the Carrizo–Wilcox aquifer in the Texas Gulf Coast Basin (Nicot 2008), the Mt. Simon aquifer in the Illinois Basin (Birkholzer et al. 2008), and saline aquifers in the Alberta Basin, Canada (Bachu et al. 1994). As the CO_2 plume spreads out under a caprock, it will become partially immobilized by capillary forces ("trapped gas"; Kumar et al. 2005), while also partially dissolving in the aqueous phase. CO_2 dissolution functions as a gateway toward potential eventual fixation of CO_2 as carbonates of low solubility, and it induces a small increase in aqueous phase density, thus alleviating concerns about upward buoyancy flow. The progression from free gas to trapped gas, dissolution into the aqueous phase, and precipitation of solid carbonates increases CO_2 storage security, and the associated quantitative aspects of CO_2 inventories and characteristic times involved are of great practical interest (IPCC 2005).

In this article, we consider the long-term evolution of a large CO_2 plume that is emplaced in a saline aquifer with a sloping caprock. We employ highly idealized descriptions of geometric and hydrogeologic parameters to focus on the role and significance of different multi-phase, multi-component flow and transport processes, including mechanisms of gas and water flow, CO_2 transport and inventory in gas and aqueous phases, and controls on the speed of advancement of the CO_2 plume. We neglect chemical interactions between CO_2 and rock minerals.

2 Definition of Reference Case

The problem is patterned after the Carrizo–Wilcox aquifer in Texas (Nicot 2008; Hesse et al. 2008). We assume that a substantial number of CO_2 storage projects will be operating in the Wilcox in a line-drive pattern perpendicular to dip, and we model a 2D vertical section along the dip of the aquifer. The aquifer is modeled as a rectangular domain of 200-m thickness and 110-km length, dipping with an angle of $\alpha = 1.5°$ against the horizontal (Fig. 1). We consider the upper right-hand corner of the domain to be at the land surface; the lower left-hand corner is then at a depth of $110{,}000\ \sin(\alpha) + 200\ \cos(\alpha)$, which for $\alpha = 1.5°$ corresponds to 3,079.4 m. Formation properties include a uniform and isotropic permeability of 500 mD, a porosity of 15%, and a compressibility of $4.5 \times 10^{-10}\ \mathrm{Pa}^{-1}$ (similar to compressibility of water at ambient conditions). The domain is initialized as a fully (fresh-)water-saturated medium in hydrostatic equilibrium, held in a geothermal gradient of 30° C/km relative to a land surface temperature of 10° C. Boundary conditions are "no flow" everywhere, except that the upper right-hand corner of the domain is held at land surface conditions of $(T_0, P_0) = (10°\ \mathrm{C}, 1.013 \times 10^5\ \mathrm{Pa})$. Temperatures and pressures increase continuously with

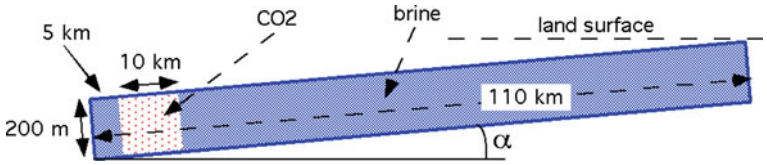

Fig. 1 2D rectangular domain modeled with geometric dimensions shown (not to scale; note the extreme aspect ratio). The domain is dipping by an angle α. The initial CO_2 plume is shown by light shading

depth, reaching values of $(T, P) = (101.83°\,\mathrm{C}, 298.15 \times 10^5\ \mathrm{Pa})$ at the lower left-hand corner.

The CO_2 plume is emplaced instantaneously with a uniform gas saturation of $S_g = 80\%$, corresponding to aqueous phase at irreducible saturation of $S_{lr} = 20\%$, to the subdomain labeled "CO_2" in Fig. 1; for the CO_2 emplacement, pressures and temperatures are maintained at their initial values. Plume evolution takes place under the combined action of gravity and pressure forces, with CO_2 buoyancy due to lower density being the primary driving force due to lower density. Thermal effects are small, and the simulation is simplified by maintaining temperatures at their initial values throughout. Effects of aqueous diffusion, and enhancement of CO_2 dissolution through convective mixing, are explored in sensitivity studies, see below. Relative permeabilities for liquid (k_{rl}) and gas (k_{rg}) were assumed as follows:

$$k_{rl} = \sqrt{S^*}\left\{1 - \left(1 - [S^*]^{1/m}\right)^m\right\}^2 \tag{1a}$$

$$k_{rg} = \left(1 - \hat{S}\right)^2\left(1 - \hat{S}^2\right) \tag{1b}$$

where $S^* = (S_l - S_{lr})/(1 - S_{lr})$, $\hat{S} = (S_l - S_{lr})/\left(1 - S_{lr} - S_{gr}\right)$, with S_l the liquid (aqueous phase) saturation, and S_{lr}, S_{gr} being the irreducible liquid and gas saturations, respectively. Equation 1a for liquid was developed by van Genuchten (1980); Eq. 1b for gas is due to Corey (1954). Parameters used are $S_{lr} = S_{gr} = 20\%$; $m = 0.457$. The relative permeabilities given by Eq. 1 are non-hysteretic; effects of hysteresis in the relative permeability functions will be explored in the future (Kumar et al. 2005; Juanes et al. 2006; Doughty 2007). For most of the simulations reported here we neglect capillary pressures, but a few cases were run with inclusion of capillary pressure effects, using the van Genuchten (1980) function in the form:

$$P_{cap} = -P_0\left([S^*]^{-1/m} - 1\right)^{1-m} \tag{2}$$

where parameters S^* and m are as above for relative permeability, while the strength parameter is chosen as $P_0 = 9.8 \times 10^3$ Pa, appropriate for reservoir rock with a permeability of 500 mD.

Obtaining accurate results for plume migration, and interpreting simulated behavior, is made difficult by the extreme aspect ratio of the flow system. This is illustrated by a contour map of densities that CO_2 would have throughout the flow domain for the applied hydrostatic–geothermal conditions, Fig. 2. Temperatures and pressures, hence CO_2 densities, are a function of depth only, and so the isolines of constant density shown in Fig. 2 are in fact horizontal. Additional difficulties arise from the multi-scale nature of the flow processes, from effects of space and time discretization, and from orders-of-magnitude variations in mass fluxes in space and time.

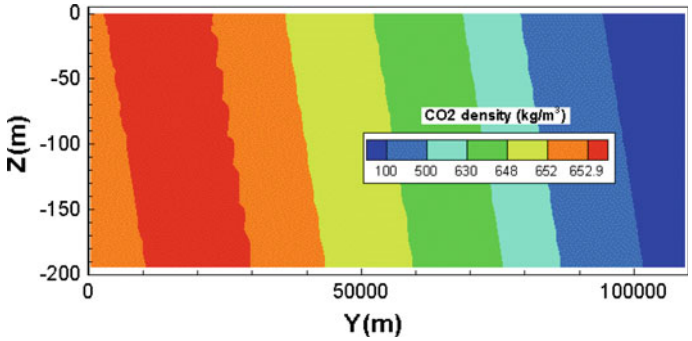

Fig. 2 Variation of the density of free-phase CO_2 throughout the model domain. Note that CO_2 density depends on temperature and pressure, both of which are a function of true depth only, so that density isolines are actually horizontal

Figure 2 shows that the interplay of temperatures and pressures both increasing with depth is such that CO_2 density is nearly constant at around $650\,\mathrm{kg/m^3}$ in the deeper portions of the aquifer. This implies that the buoyancy force experienced by CO_2 in a hydrostatic pressure field is nearly the same throughout the deeper regions. Only for $Y > 70\,\mathrm{km}$, corresponding to true depths less than 1,047 m, is CO_2 becoming noticeably less dense. As will be seen below, CO_2 flow effects produce only modest perturbations of the initial hydrostatic pressure field, so that the CO_2 densities plotted in Fig. 2 and the buoyancy forces associated with them are relevant for the actual plume evolution.

CO_2 was introduced into the 10 km by 200-m-large domain highlighted in Fig. 1 under conditions corresponding to the initial hydrostatic pressure equilibrium in a geothermal gradient. Owing to its lower density as compared to aqueous phase, CO_2 experiences a buoyancy force that drives it upward, toward shallower depth. The evolution of the CO_2 plume was modeled with a parallelized version TOUGH2-MP of our general-purpose reservoir simulator TOUGH2 (Pruess 2004; Zhang et al. 2008), augmented with a fluid property module ECO2N that provides accurate correlations for thermophysical properties of fluids, including the partitioning of H_2O and CO_2 between brine and gas phases (Pruess and Spycher 2007). The basic space discretization was 10 m in the sub-vertical and 1,000 m in the sub-horizontal direction, but we did some experimentation with grid refinement to achieve a compromise between spatial resolution and efficient execution. The simulations presented here were performed with a grid that involved refinement to $\Delta Z = 1\,\mathrm{m}$ near the top, to better resolve the CO_2 plume, as well as refinement to $\Delta Y = 10\,\mathrm{m}$ in the (sub-) horizontal direction near $Y = 50\,\mathrm{km}$; the total number of grid blocks is 7,300. The horizontal refinement was done to be able to monitor up–dip plume advancement with a spatial resolution down to 10 m, albeit in a region of limited lateral extent, and thereby obtain a more accurate depiction and understanding of flow mechanisms at the advancing phase front. The simulations were run on a Dell T5400 dual quad core computer with a total of eight cores. For parallelized execution, we would normally partition the simulation domain into an equal number of subdomains (8), and assign each processor core the computations corresponding to one subdomain. However, in most cases, we partitioned the computations into 16 parallel processes (two per processor), as this was found to reduce execution time compared to running eight processes. Individual runs typically took about 1–1.5 h.

3 Plume Migration

Figure 3 shows gas saturations at three different times, from early to late, and indicates strong gravity override as the plume migrates up–dip near the top of the permeable interval. The plume thins out as it migrates under the sloping caprock, and mass flows of CO_2 generally decrease with time and distance from the original CO_2 emplacement. One might expect that the advancement of the plume may slow over time also, but this is not the case. Figure 4 shows that the plume does advance more rapidly for a brief initial period, because of the strong driving force provided by the initial placement of the CO_2 plume in a hydrostatic pressure field. However, subsequent advancement of the plume occurs with constant speed. From the slope of the eye-fitted straight line, we deduce an average speed of plume advancement of $V_p = 5.41 \times 10^{-6}$ m/s (170.7 m/year). The speed of plume advancement is the same as the pore velocity of CO_2 at the front. Its near-constancy can be understood by noting that (1) gas saturations are nearly constant throughout at $S_g \approx 73\%$ in the upper portions of the plume (Fig. 5), (2) the pressure field remains close to hydrostatic (Fig. 6), and (3) CO_2 density, hence buoyancy force in a given pressure gradient, varies only weakly with position (Fig. 2).

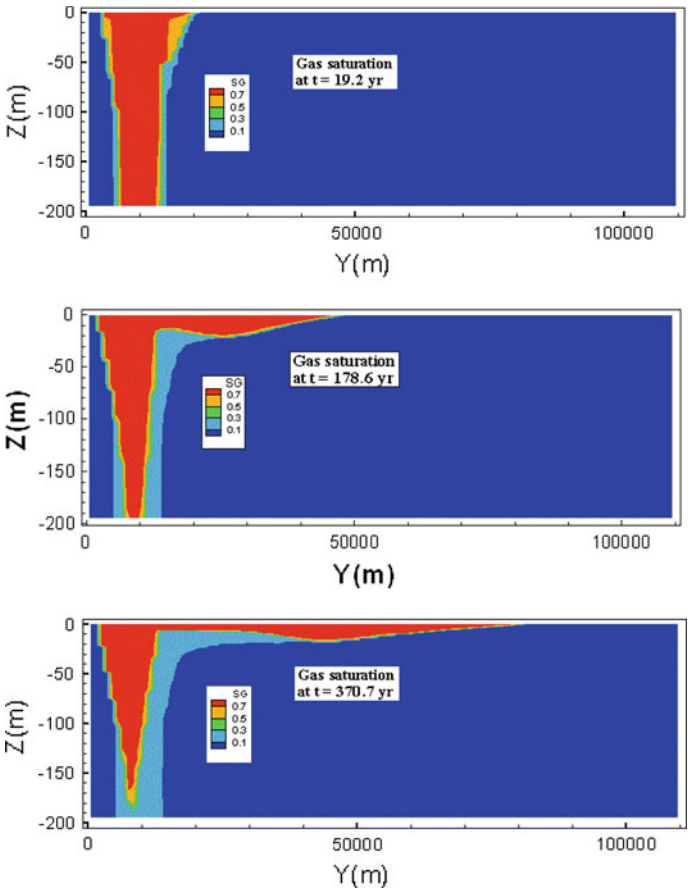

Fig. 3 Simulated gas saturations at different times

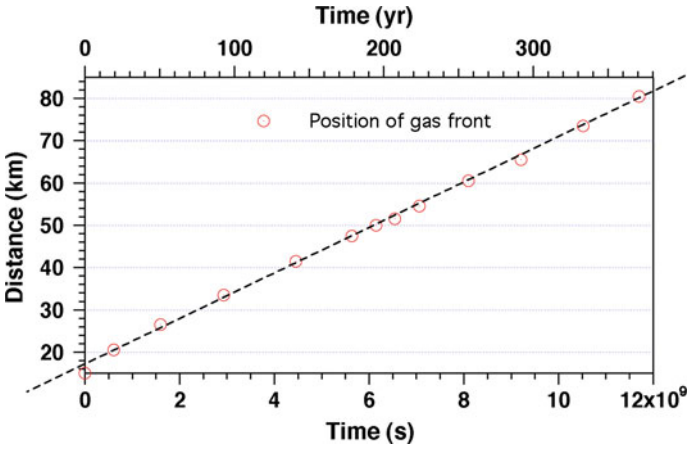

Fig. 4 Advancement of the gas front over time. Distance is measured with respect to the l.h.s. of the domain, so that at time $t = 0$, the plume extends to $Y = 15$ km. The dashed straight line is an eye-fit to the data

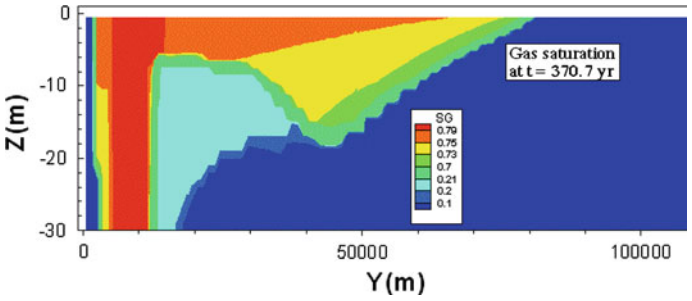

Fig. 5 Detailed view of gas saturations near the top boundary. Note the extreme vertical exaggeration

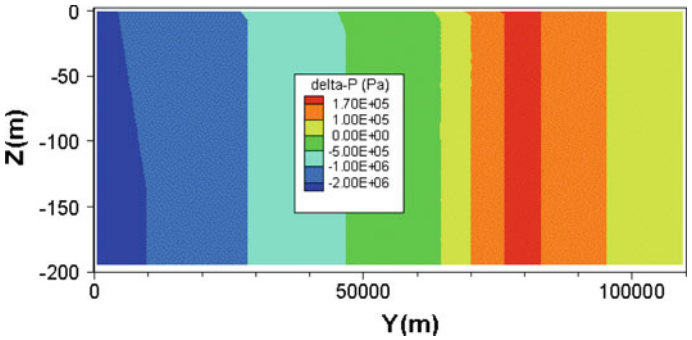

Fig. 6 Simulated pressure changes over a period of 370.7 years

The simulated result for plume migration speed can be quantitatively explained by considering the motion of an immiscible plume of CO_2 with density difference $\Delta\rho$ relative to the surrounding aqueous phase in a hydrostatic pressure field. The volumetric flux associated with the rise of such a plume would be given by $u = k\left(k_{\mathrm{rg}}/\mu_{\mathrm{g}}\right)\Delta\rho\, g$, and the com-

Table 1 Data used for evaluating pore velocity from buoyancy flow from Eq. 3

Permeability	$k = 500 \times 10^{-15}\ \mathrm{m}^2$
Porosity	$\phi = 15\%$
Gas saturation in plume	$S_g = 73\%$
Gas relative permeability from Eq. 1b	$k_{rg}(S_g{=}0.73) = 0.77$
Gas phase viscosity at (T, P) = (55°C, 150 bar)[a]	$\mu_g = 0.525 \times 10^{-4}$ Pa-s
Gas density at (T, P) = (55°C, 150 bar)[a]	$\rho_g = 654.96\,\mathrm{kg/m}^3$
Water density at (T, P) = (55°C, 150 bar)[a]	$\rho_l = 992.14\,\mathrm{kg/m}^3$
Density difference[a]	$\Delta\rho = 337.18\,\mathrm{kg/m}^3$
Tilt	$\sin\theta = \sin 1.5° = 0.02618$
Gravitational acceleration	$g = 9.81\,\mathrm{m/s}^2$

[a] Corresponding to conditions at approximately 1,500 m depth

ponent along the slope of a caprock tilted by an angle θ would be $u \sin\theta$. The corresponding pore velocity would be

$$V_{\mathrm{pore}} = \frac{u \sin\theta}{\phi S_g} = \frac{k k_{rg} \Delta\rho\, g}{\phi S_g \mu_g} \sin\theta \tag{3}$$

Inserting applicable parameters from Table 1 yields $V_{\mathrm{pore}} = 183.0$ m/year, in excellent agreement with the value of 170.7 m/year read off the slope of the straight line in Fig. 4. Hesse et al. (2008) performed a detailed analysis of plume migration in a vertically averaged sharp interface model, which for the advancement of the plume tip reduces to Eq. 3. However, the model of Hesse et al. assumes a gas saturation of $S_g = 1 - S_{lr}$ throughout the plume, or $S_g = 80\%$ for the parameters used here. This results in a gas relative permeability that is about 30% larger than for $S_g \approx 73\%$ obtained in our simulation, so that the speed of plume advancement predicted from the theory of Hesse et al. (2008) is then somewhat larger also, namely 216.9 m/year.

To further understand the relationship between the 2D simulations and vertical equilibrium, sharp interface, models, we ran a simple 1D simulation using a vertically averaged two-phase model. Here, we fixed the flow parameters according to Table 1 and Eqs. 1a, b throughout the system, thus neglecting the variation of viscosity and density in the domain. The result, using high resolution numerics to ensure a converged solution, is shown after 370.7 years in Fig. 7. Here, mobile phase CO_2 ($S_g = 0.73$) is shown in dark gray, and the region with irreducible CO_2 saturation ($S_g = 0.20$) is shown in light gray. From the figure, we see that the vertically equilibrated model gives excellent qualitative agreement with the 2D simulation shown in Fig. 3 (bottom panel). The plume tip has reached a distance of 88 km, as compared to 80.5 km in the 2D simulation (Fig. 4). Unlike Hesse et al. (2008) and Juanes et al. (2010), we have accounted for the reduced relative permeability of brine at the irreducible saturation of CO_2 (see e.g., Lake 1989; Nordbotten and Dahle 2011). Without this detailed treatment of brine flow in the 1D model, the slowly depleting bank of CO_2 seen in the 2D model cannot be reproduced with a 1D model. We make two notes regarding the quantitative interpretation of the 1D model: First, the tip speed predicted by Eq. 3 is reproduced exactly by the late time limit for the vertically integrated model. However, at earlier, and indeed relevant, times, dispersive terms lead to a higher tip speed. The value of Eq. 3 as a rough estimator of plume speed, as observed from the fully resolved simulations, is thus also supported by vertically integrated models. Second, the vertically integrated model can be extended to include variation in fluid properties. This is beyond the scope of this study, but would allow us to make direct quantitative comparisons between the 1D and 2D models.

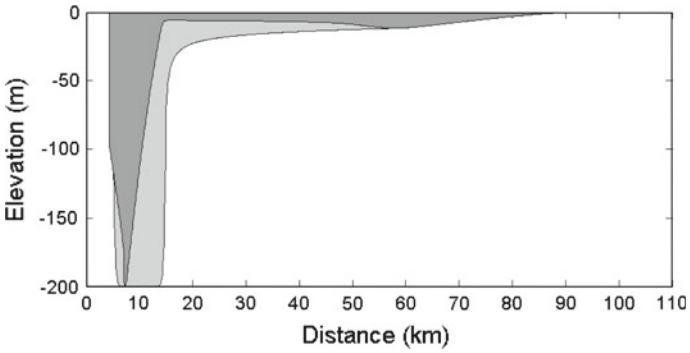

Fig. 7 CO_2 saturations after $t = 370.7$ years obtained from a vertically integrated sharp-interface model. The lightly shaded region has gas saturations $S_g \geq 0.2$, while the dark shading indicates gas saturations $S_g \geq 0.73$. Plume tip is at 88-km distance

The nearly constant gas phase density together with nearly constant pore velocity further implies that the up–dip CO_2 mass flux is nearly independent of position and time. Accordingly, the total CO_2 mass flow rate in the direction of plume migration must decrease in proportion to the plume thickness. Figure 5 also indicates that the thickness of the plume behind the tip, hence the total CO_2 mass flow rate, increases approximately linearly with distance from the tip. At larger distance behind the plume tip, the thickness of the mobile plume is reduced, and beneath the mobile portion is a region of considerable thickness in which gas saturation is near the irreducible limit of 0.2 (Fig. 5). This region had been swept by CO_2 at earlier time, and subsequently has been depleted of mobile CO_2 by slow upflow in a vertical gradient that is intermediate between gas-static and hydrostatic.

4 Behavior of Aqueous Phase

The aqueous phase plays a four-fold role in affecting the evolution of the CO_2 plume, (1) it serves as a medium for pressure transmission, (2) it occupies pore space that must be vacated to enable advancement of the CO_2 plume, (3) it can dissolve CO_2, thus serving as a sink, and (4) it serves as a transport medium for dissolved CO_2 by diffusive and advective processes.

Figure 8 shows a snapshot of water pore velocities at $t = 6.147 \times 10^9$ s (194.8 year), at which time the gas plume has advanced to $Y = 50$ km (Fig. 4). The reason for picking a snapshot at this particular time is that we have applied local grid refinement around $Y = 50$ km, making this a "preferred spot" for understanding water flow. It is seen that there are large downward water velocities right at and beneath the gas front, which can be understood as follows. Owing to the lower density and large mobility of CO_2, vertical pressure gradients are near CO_2-static and less than hydrostatic throughout the plume. Water near the plume tip thus experiences a less-than-hydrostatic gradient, causing water to flow downward, and vacating pore space at the top of the permeable interval into which the CO_2 plume may advance. A more detailed analysis available in a laboratory report (Pruess 2009) shows that integrating the simulated downward aqueous phase flux over time quantitatively accounts for the voidage of pore space and increase in gas saturation at the plume tip. Thus, water is removed at the advancing gas front primarily by downward rather than by outward flow, and one may say that the groundwater column "collapses" upon approach of the CO_2 plume with its smaller vertical pressure gradient. This mechanism of gas invasion into the aqueous zone is quite different from what would be encountered near a CO_2 injection well, where a

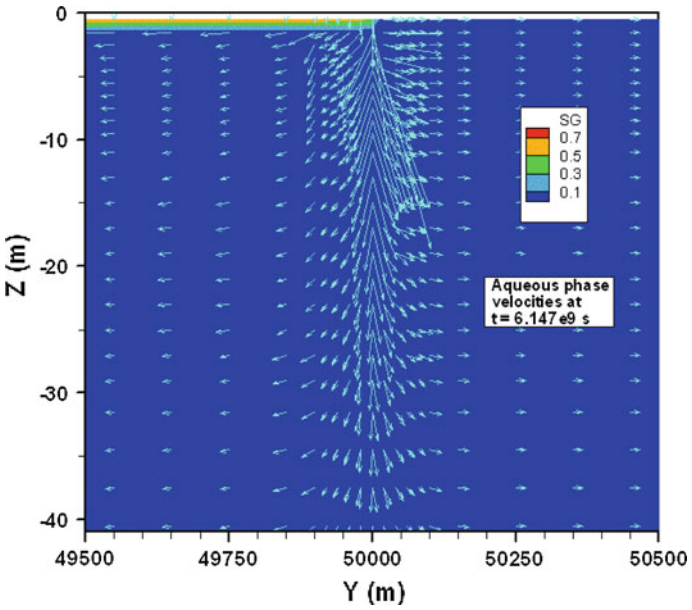

Fig. 8 Aqueous phase velocities near the gas front at time $t = 194.8$ year. The lengths of vectors are proportional to velocity

gas plume will advance by displacing water outward under a pressure gradient maintained by the injection operation (Pruess and Müller 2009). The downward water flow generates a flow divide in the aqueous phase, where behind the gas front aqueous phase flows downward and inward, while beyond the gas front water flow is downward and outward, away from the plume. In the plume itself, water flow is small and downward.

The observation of the crucial role of vertical liquid flow for the up–dip migration of CO_2 suggests that reducing the permeability for downward water flow should reduce the speed of plume advancement. Results presented in Fig. 9 show that this is indeed the case. Simulations in which vertical permeability to liquid was reduced by factors of 10 and 100 yield smaller speeds of $V_p = 4.25 \times 10^{-6}$ m/s (134.1 m/year) and 2.65×10^{-6} m/s (83.6 m/year), respectively, as compared to the isotropic case with $V_p = 5.41 \times 10^{-6}$ m/s (170.7 m/year). The speeds were obtained as the slopes of straight lines that were eye-fitted to the data labeled $k_{v,liq}/k_h = 0.1$ and 0.01 in Fig. 9. Applying the same reduction factor for vertical permeability to gas as well (curves labeled $k_v/k_h = 0.1$ and 0.01 in Fig. 9) does not have any additional impact on the speed of plume advancement, confirming the essential role of downward aqueous phase flow in controlling the up–dip migration of the CO_2 plume. We note that effects of vertical aqueous phase flow are ignored in vertical equilibrium models of CO_2 plume migration such as (Hesse et al. 2008; Juanes et al. 2010), which will cause such models to overpredict the speed of up–dip plume advancement. That vertical equilibrium (VE) models will eventually break down when vertical permeability k_v becomes small is expected from the theoretical analysis of Yortsos (1995) who showed that the VE model arises as the leading order term in an asymptotic expansion with respect to the parameter $r = (H/L)\sqrt{k_h/k_v}$, where H and L are the reservoir thickness and length, respectively. Reducing k_v will increase the parameter r and will make higher-order terms beyond the VE approximation more important.

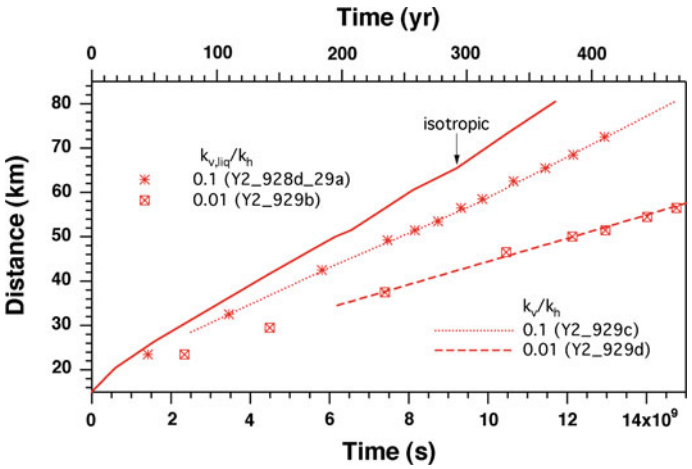

Fig. 9 Simulated advancement of the CO_2 plume for an isotropic medium (same as Fig. 4), compared with systems in which vertical permeability was reduced for liquid phase only ($k_{\mathrm{v,liq}}/k_{\mathrm{h}} \leq 0.1$), or for both phases ($k_{\mathrm{v}}/k_{\mathrm{h}} \leq 0.1$)

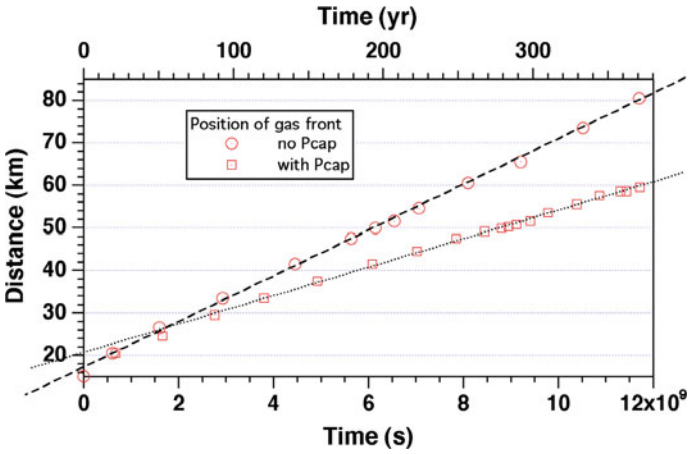

Fig. 10 Simulated plume advancement with and without inclusion of capillary pressures

There are other effects that may affect the movement of the aqueous phase and thereby alter the speed of plume advancement. Capillary pressures will exert a force that will draw the aqueous phase toward the plume. This will impede the downward drainage of aqueous phase, and is thus expected to reduce the speed of plume advancement. Figure 10 shows that this is indeed the case; capillary effects reduce the plume migration speed from 170.7 m/year to 105.3 m/year. In the simulation studies presented here, the formation fluid was represented as fresh water; salinity of formation water is also expected to reduce the plume migration speed, as it will increase the viscosity and reduce the mobility of the aqueous phase. This effect has not yet been explored; it may be (partially) compensated by the increase in the density of the aqueous phase due to salinity, which will increase the buoyancy force on CO_2.

5 Dissolution of CO_2

The initial CO_2 inventory in the flow domain is 158.7 kt (for a section of 1-m thickness), of which only about 3.1 kt (2.0%) is dissolved in the aqueous phase. Equilibrium dissolved CO_2 mass fraction is approximately 5.2% throughout most of the flow domain. With a total initial aqueous phase inventory of 3.03×10^9 kg, dissolution equilibrium would correspond to a total amount of dissolved CO_2 of 157.6×10^6 kg = 157.6 kt, which is almost exactly equal to the total initial CO_2 inventory. This indicates that the aqueous phase represents a very large sink, that potentially can dissolve almost the entire CO_2 inventory. The critical issue is, how readily is this sink available, i.e., how fast is dissolution occurring? Over time, the dissolved CO_2 inventory increases, reaching 14.2 kt, or 9.0% of the total, after 13.18×10^9 s (417.7 year; see Fig. 11). Figure 11 also shows free phase and dissolved CO_2 inventories for a simulation in which molecular diffusion of CO_2 in the aqueous phase was taken into account. Diffusion will transport CO_2 away from the interface between aqueous and gas phases, thus providing a mechanism for solubilizing additional CO_2. The diffusivity of CO_2 for the pressure and temperature conditions of interest here is approximately $D = 2 \times 10^{-9}\,\mathrm{m}^2/\mathrm{s}$ (Tewes and Boury 2005; Farajzadeh 2009); our simulation includes porous medium tortuosity effects and uses an effective diffusivity of $D_{\mathrm{eff}} = 1 \times 10^{-9}\,\mathrm{m}^2/\mathrm{s}$. However, Fig. 11 shows that aqueous diffusion has very small effects and leads to only a slight increase in dissolved CO_2. Diffusion is a slow process, and after 300 years ($= 9.5 \times 10^9$ s) would penetrate a distance of only $L = \sqrt{D_{\mathrm{eff}} t} = \sqrt{9.5} = 3.1$ m into the aqueous phase.

There is another effect from CO_2 dissolution and subsequent diffusion, which has been neglected in the simulations presented above, and that can potentially make much larger contributions to solubilizing CO_2. Dissolution of CO_2 into aqueous phase induces an increase in aqueous phase density that, depending on salinity, is typically ranging from 1% (for pure water) to 0.1% (for highly saline brine). Although small, this density increase gives rise to a gravitationally unstable configuration of denser fluid above less-dense fluid. This can induce convection in the aqueous phase, which can transport CO_2 downward, away from the dissolution boundary, at much larger rates than molecular diffusion. Because of its potential relevance for accelerating CO_2 dissolution, the process of dissolution–diffusion–convection

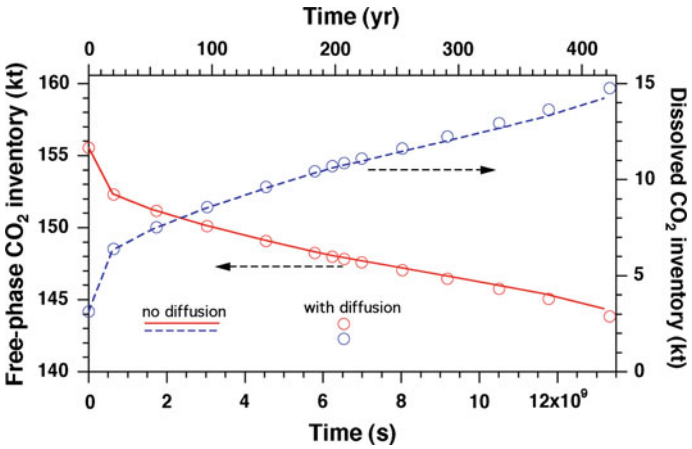

Fig. 11 Time dependence of free-phase and dissolved CO_2 inventory

(DDC) has been studied by many investigators (Lindeberg and Bergmo 2003; Ennis-King and Paterson 2003a,b, 2005; Ennis-King et al. 2005; Hesse et al. 2006; Riaz et al. 2006; Xu et al. 2006; Rapaka et al. 2008; Pruess and Zhang 2008; Kneafsey and Pruess 2010; Pau et al. 2010). Most studies have focused on analyzing the convective instability for idealized geometries and parameters, to determine the onset or incubation time $t_{\rm inc}$ required for convection to start, and the corresponding thickness $L_{\rm inc}$ at which the diffusive boundary layer becomes unstable. Even though our simulations properly account for increase in aqueous phase density from CO_2 dissolution, they do not generate any buoyancy-driven aqueous phase convection over the time period simulated. This is because the development of such convection is suppressed by the relatively coarse gridding in our field-scale model.

We have performed high-resolution simulations of the DDC process, using a 1 m wide by 5 m tall rectangular domain (Pruess and Zhang 2008). Vertical grid resolution was 1 mm near the top of the domain, gradually coarsening to 1 cm at larger distance from the boundary; horizontal resolution was 1 cm. The computational mesh has 52,300 grid blocks with 104,500 connections. Typical run times on a Dell T5400 dual quad core computer are approximately 7 h. By comparing CO_2 mass transfer rates with an analytic solution for diffusion only, we deduce an incubation time of 4.0×10^6 s for onset of convective activity, and a stabilized long-term convectively enhanced CO_2 dissolution rate due to DDC of approximately 1.0×10^{-7}kg/s/m^2 (Fig. 12). Accordingly, the enhanced dissolution process will start practically instantaneously relative to characteristic time scales of plume migration.

What ramifications can be expected from accelerated CO_2 dissolution for the long-term behavior of the plume? The simulations presented above showed that gas saturations and up–dip CO_2 fluxes in the mobile (upper) part of the plume are approximately constant, independent of space and time. This holds true even though plume thickness is a complicated function of time and distance, and it is the reason why the plume advances with constant speed. On the basis of these findings, we expect that accelerated dissolution will reduce the thickness of the plume, but will have little impact on gas saturations and CO_2 fluxes in the upper, mobile portion of the plume. Accordingly, we hypothesize that the speed of plume advancement will be unaffected by accelerated dissolution from DDC.

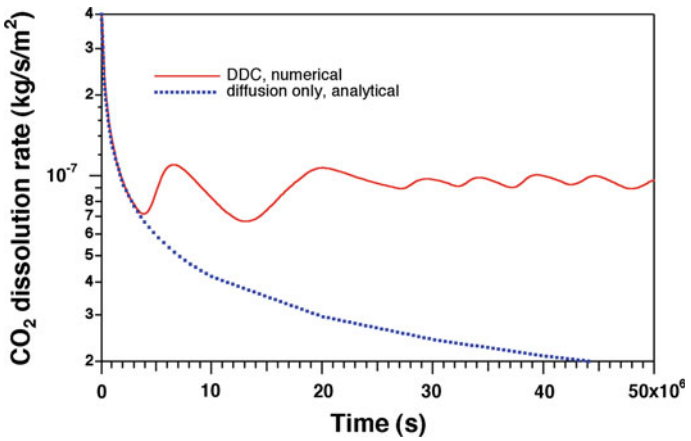

Fig. 12 CO_2 dissolution rate due to convective enhancement, obtained from high-resolution simulations

This hypothesis was tested by implementing a first, admittedly crude model of sub-grid-scale DDC into TOUGH2-MP. Our approach represents enhanced CO_2 dissolution by means of a sink term applied to the region with free-phase CO_2. The DDC process is expected to remove free-phase CO_2 primarily from the lower portions of the CO_2 plume, near the boundary between two-phase fluid above and a single aqueous phase below. This boundary is time dependent, and gas phase saturations immediately above the boundary are small over much of the plume, near the irreducible limit of $S_{gr} = 20\%$, raising significant issues for incorporating a dynamic, self-consistent DDC sink into a numerical model. We avoid these issues by adopting a highly simplified model that applies the DDC sink to the top row of grid blocks throughout the entire region with two-phase conditions. This will overestimate effects of dissolution on the mobile part of the plume, and therefore should overestimate the reduction in the speed of plume advancement from DDC, if indeed any such reduction occurs. Other approximations invoked in our model for sub-grid-scale enhanced dissolution include neglecting the (small) incubation time for onset of convection; assuming convective

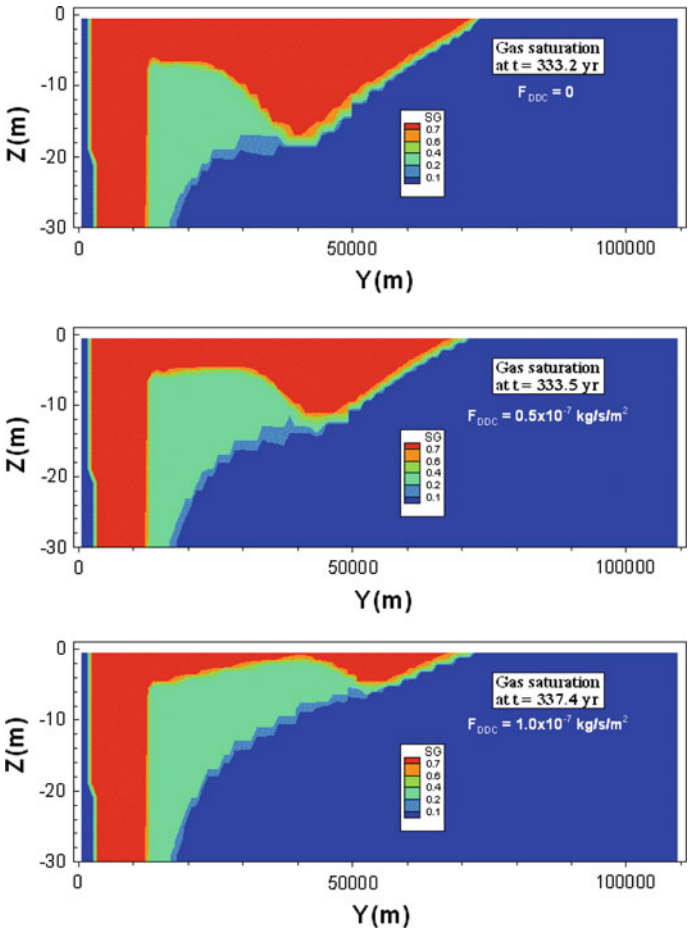

Fig. 13 Gas saturations after approximately 335 years, for different strengths of convectively enhanced CO_2 dissolution rates

CO_2 flux to be constant, independent of time; applying a threshold criterion of $S_g > 20\%$ before turning on DDC in a grid block; and lagging DDC flux by one time step.

Simulations of plume migration subject to DDC were performed for two different values of the dissolution flux, $F_{DDC} = 1 \times 10^{-7}$ kg/s/m^2 as determined in our fine-grid simulation (Fig. 12), and a value half this large, $F_{DDC} = 0.5 \times 10^{-7}$kg/s/m^2, to explore the sensitivity to reduced vertical permeability. Figure 13 compares results for the CO_2 plumes after about 335 years with the previous simulation that ignored DDC. As had been expected, the main effect of enhanced dissolution is to reduce the thickness of the upper, highly mobile portions of the plume, while impacts on the advancement of the plume appear to be minor. A plot of plume advancement versus time indeed shows that plume advancement is essentially unaffected by CO_2 solubilization due to DDC (Fig. 14). There is a very minor reduction in plume speed at intermediate times, which probably is due to space discretization effects from the $\Delta Z = 1$ m grid resolution at the top boundary. Finding little evidence for reduction in

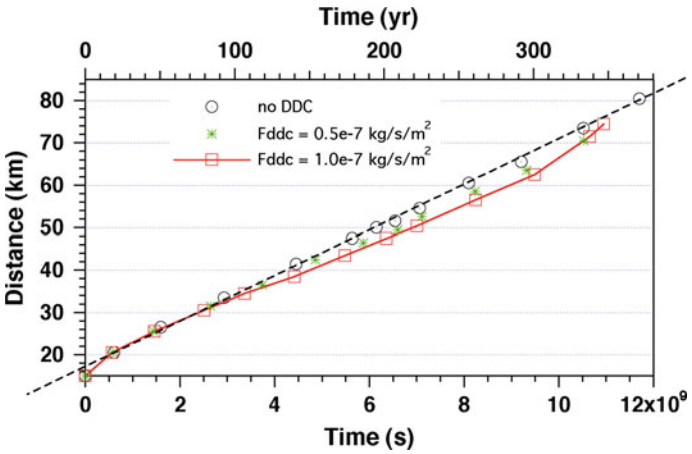

Fig. 14 Plume advancement versus time for different convectively enhanced CO_2 dissolution rates

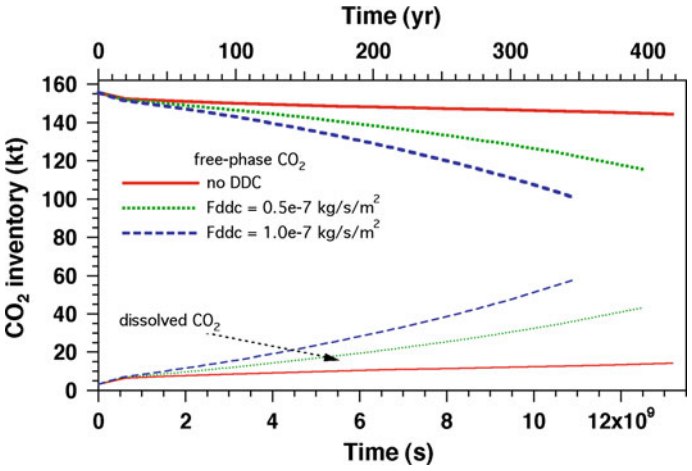

Fig. 15 Free-phase and dissolved CO_2 inventories for different CO_2 dissolution rates

the speed of plume advancement even when making an approximation that would overestimate such effects indicates that, for the particular problem specifications investigated here, plume advancement indeed is essentially unaffected by convectively enhanced dissolution. However, we expect that a different outcome could be possible for different problem parameters that would alter the relative rates of CO_2 upflow versus convectively enhanced dissolution. Indeed, if with increasing plume footprint the rate at which free-phase CO_2 is removed from the plume would catch up with the total rate of updip CO_2 flow, then we would expect plume advancement to eventually come to a stop.

Mass balances for free-phase and dissolved CO_2 show substantial increase in CO_2 solubilization from DDC (Fig. 15). In plotting Fig. 15, we included the free-phase CO_2 removed by our sub-grid-scale representation of DDC as dissolved CO_2. For the case with $F_{\mathrm{DDC}} = 1 \times 10^{-7}\,\mathrm{kg/s/m^2}$, at the end of the simulation (340 years) approximately 1/3 of the initial CO_2 inventory has been dissolved into the aqueous phase, while 2/3 remain as a free supercritical phase.

6 Concluding Remarks

The migration of a CO_2 plume under a sloping caprock involves processes on a wide range of space and time scales, and poses difficult challenges for numerical modeling. We have used the TOUGH2-MP/ECO2N simulator on a plume migration problem with parameters applicable to the Carrizo–Wilcox aquifer in Texas. Plume behavior was simulated for time scales of a few hundred years, and covering a migration distance of order 100 km. In addition, we performed high-resolution simulations of the convective instability that develops when CO_2 dissolves and diffuses into aqueous phase, increasing fluid density, and inducing convectively enhanced CO_2 dissolution. Our main findings are as follows:

- Gas saturations in the advancing CO_2 plume are nearly uniform, and up–dip migration occurs at constant speed, independent of plume thickness.
- The mechanism of plume advancement is quite different from displacement behavior in the vicinity of an injection well. Near an injection well, the CO_2 plume advances by pressure-driven displacement of aqueous phase away from the injection point (Pruess and Müller 2009). In contrast, at the tip of a CO_2 plume advancing under a sloping caprock, water flow is mostly downward rather than outward. The plume advances up–dip because of a collapse of the groundwater column ahead of the plume tip, induced by the approaching smaller (near CO_2-static) vertical pressure gradient in the CO_2 plume.
- The speed of up–dip plume advancement is slower in an anisotropic medium with lower vertical than horizontal permeability, due to the added resistance to downward liquid flow. These effects are not captured in recent vertical equilibrium models (Hesse et al. 2008; Juanes et al. 2010).
- In a coarsely gridded field-scale model, the process of dissolution and diffusion of CO_2 into the aqueous phase does not give rise to convective mixing, because the large scale of spatial averaging suppresses the convective instability.
- High-resolution simulations show that the process of CO_2 dissolution-diffusion-convection (DDC) gives rise to CO_2 dissolution at an enhanced rate that stabilizes over time.
- A first rough model for subgrid-scale DDC was implemented into our TOUGH2-MP code, and was used to explore the impact of DDC on long-term behavior of the plume. The results showed that enhanced dissolution made the advancing CO_2 plume thinner and reduced the up–dip CO_2 flow rate, but did not affect the speed of plume advancement.

Future work will need to address the effects neglected in this study, including formation heterogeneities, salinity of formation fluids, hysteresis in relative permeability functions (Doughty 2007), and chemical interactions induced by injected CO_2.

Acknowledgments Thanks are due to Curt Oldenburg and Christine Doughty for their careful reviews of the manuscript and the suggestions of improvements. This study was supported by the Office of Basic Energy Sciences under Contract No. DE-AC02-05CH11231 with the U.S. Department of Energy, and by Norwegian Research Council grant 180679, "Modelling Transport in Porous Media over Multiple Scales."

References

Bachu, S., Gunter, W.D., Perkins, E.H.: Aquifer disposal of CO_2: hydrodynamic and mineral trapping. Energy Convers. Manag. **35**, 269–279 (1994)

Birkholzer, J.T., Zhou, Q., Tsang, C.-F.: Large-scale impact of CO_2 storage in deep saline aquifers: a sensitivity study on the pressure response in stratified systems. Int. J. Greenh. Gas Control (2008). doi:10.1016/j.ijggc.2008.08.002

Celia, M.A., Nordbotten, J.M., Bachu, S., Dobossy, M., Court, B.: Risk of leakage versus depth of injection in geological storage. In: Proceedings, 9th International Conference on Greenhouse Gas Control Technologies, Washington, D.C., November (2008)

Corey, A.T.: The interrelation between gas and oil relative permeabilities. Producers Monthly, pp. 38–41, November (1954)

Doughty, C.: Modeling geologic storage of carbon dioxide: comparison of non-hysteretic and hysteretic characteristic curves. Energy Convers. Manag. **48**, 1768–1781 (2007)

Ennis-King, J., Paterson, L.: Rate of dissolution due to convective mixing in the underground storage of carbon dioxide. In: Gale, J., Kaya, Y. (eds.) Greenhouse Gas Control Technologies, Volume 1, pp. 507–510. Elsevier, Amsterdam (2003a)

Ennis-King, J., Paterson, L.: Role of convective mixing in the long-term storage of carbon dioxide in deep saline formations. In: paper SPE-84344, presented at Society of Petroleum Engineers Annual Fall Technical Conference and Exhibition, Denver, CO, October (2003b)

Ennis-King, J., Paterson, L.: Role of convective mixing in the long-term storage of carbon dioxide in deep saline formations. SPE J. 349–356 (2005)

Ennis-King, J., Preston, I., Paterson, L.: Onset of convection in anisotropic porous media subject to a rapid change in boundary conditions. Phys. Fluids **17**, 084107 (2005). doi:10.1063/1.2033911

Farajzadeh, R.: Enhanced transport phenomena in CO_2 sequestration and CO_2 EOR, PhD thesis, Technical University Delft, The Netherlands (2009)

Hesse, M.A., Tchelepi, H.A., Orr, F.M. Jr.: Natural convection during aquifer CO_2 storage. In: presented at GHGT-8, 8th International Conference on Greenhouse Gas Control Technologies. Trondheim, Norway, June (2006)

Hesse, M.A., Orr, F.M. Jr., Tchelepi, H.A.: Gravity currents with residual trapping. J. Fluid Mech. **611**, 35–60 (2008)

IPCC (Intergovernmental Panel on Climate Change): Special Report on Carbon Dioxide Capture and Storage (2005)

Juanes, R., Spiteri, E.J., Orr, F.M. Jr., Blunt, M.J.: Impact of relative permeability hysteresis on geological CO_2 storage. Water Resour. Res. **42**, W12418 (2006). doi:10.1029/2005WR004806

Juanes, R., MacMinn, C.W., Szulczewski, M.L.: The footprint of the CO_2 plume during carbon dioxide storage in saline aquifers: storage efficiency for capillary trapping at the basin scale. Transp. Porous Media **82**(1), 19–30 (2010)

Kneafsey, T.J., Pruess, K.: Laboratory flow experiments for visualizing carbon dioxide-induced, density-driven brine convection. Transp. Porous Media **82**(1), 123–139 (2010). doi:10.1007/s11242-009-9482-2

Kumar, A., Ozah, R., Noh, M., Pope, G.A., Bryant, S., Sepehrnoori, K., Lake, L.W.: Reservoir simulation of CO_2 storage in deep saline aquifers. SPE J **10**(3), 336–348 (2005)

Lake, L.W.: Enhanced Oil Recovery. Prentice-Hall, Englewood Cliffs (1989)

Lindeberg, E., Bergmo, P.: The long-term fate of CO_2 injected into an aquifer. In: Gale, J., Kaya, Y. (eds.) Greenhouse Gas Control Technologies, pp. 489–494. Elsevier Science, Ltd., Amsterdam, The Netherlands (2003)

Nicot, J.-P.: Evaluation of large-scale CO_2 storage on fresh-water sections of aquifers: an example from the Texas Gulf Coast Basin. Int. J. Greenh. Gas Control **2**(4), 583–593 (2008)

Nordbotten, J.M., Celia, M.A., Bachu, S., Dahle, H.K.: Semianalytical solution for CO_2 leakage through an abandoned well. Environ. Sci. Technol. **39**(2), 602–611 (2005). doi:10.1021/es035338i

Nordbotten, J.M., Dahle, H.K.: Impact of the capillary fringe in vertically integrated models for CO_2 storage. Water Resour. Res. doi:10.1029/2009WR008958 (2011)

Pau, G.H.S., Bell, J.B., Pruess, K., Almgren, A.S., Lijewski, M.J., Zhang, K.: High resolution simulation and characterization of density-driven flow in CO_2 storage in saline aquifers. Adv. Water Res. (2010). doi:10.1016/j.advwatres.2010.01.009

Pruess, K.: The TOUGH Codes—a family of simulation tools for multiphase flow and transport processes in permeable media. Vadose Zone J. **3**, 738–746 (2004)

Pruess, K.: On CO_2 fluid flow and heat transfer behavior in the subsurface, following leakage from a geologic storage reservoir. Env. Geol. **54**(8), 1677–1686 (2008). doi:10.1007/s00254-007-0945-x

Pruess, K.: Numerical simulation experiments on the long-term evolution of a CO_2 plume under a sloping caprock, Lawrence Berkeley National Laboratory Report LBNL-2542E, September (2009)

Pruess, K., Müller, N.: Formation dry-out from CO_2 injection into saline aquifers: 1. Effects of solids precipitation and their mitigation. Water Resour. Res. **45**, W03402 (2009). doi:10.1029/2008WR007101

Pruess, K., Spycher, N.: ECO2N—a fluid property module for the TOUGH2 code for studies of CO_2 storage in saline aquifers. Energy Convers. Manag. **48**(6), 1761–1767 (2007). doi:10.1016/j.enconman.2007.01.016

Pruess, K., Zhang, K.: Numerical modeling studies of the dissolution–diffusion–convection process during CO_2 storage in saline aquifers, Lawrence Berkeley National Laboratory Report LBNL-1243E, November (2008)

Rapaka, S., Chen, S., Pawar, R.J., Stauffer, P.H., Zhang, D.: Non-modal growth of perturbations in density-driven convection in porous media. J. Fluid Mech. **609**, 285–303 (2008)

Riaz, A., Hesse, M., Tchelepi, H.A., Orr, F.M. Jr..: Onset of convection in a gravitationally unstable diffusive boundary layer in porous media. J. Fluid Mech. **548**, 87–111 (2006)

Tewes, F., Boury, F.: Formation and rheological properties of the supercritical CO_2–Water Pure Interface. J. Phys. Chem. B **109**(9), 3990–3997 (2005)

van Genuchten, M.Th.: A closed-form equation for predicting the hydraulic conductivity of unsaturated soils. Soil Sci. Soc. Am. J. **44**, 892–898 (1980)

Xu, X., Chen, S., Zhang, D.: Convective stability analysis of the long-term storage of carbon dioxide in deep saline aquifers. Adv. Water Resour. **29**, 397–407 (2006)

Yortsos, Y.C.: A theoretical analysis of vertical flow equilibrium. Transp. Porous Media **18**, 107–129 (1995)

Zhang, K., Wu, Y.S., Pruess, K.: User's guide for TOUGH2-MP–a massively parallel version of the TOUGH2 code, Lawrence Berkeley National Laboratory Report LBNL-315E, May (2008)